Ore Geology Reviews 115 (2019) 103178

Contents lists available at ScienceDirect

Ore Geology Reviews

journal homepage: www.elsevier.com/locate/oregeorev

Low-temperature thermochronology of the Carlin-type gold deposits in southwestern Guizhou, China: Implications for mineralization age and geological thermal events

Yong Huang[a,b], Ruizhong Hu[a,b,*], Xianwu Bi[a], Shanling Fu[a], Keqiang Peng[a,b], Wei Gao[a], Abiola Oyebamiji[a,b], Aizat Zhaanbaeva[a,b]

[a] State Key Laboratory of Ore Deposit Geochemistry, Institute of Geochemistry, Chinese Academy of Sciences, Guiyang 550081, China
[b] College of Earth and Planetary Sciences, University of Chinese Academy of Sciences, Beijing 100049, China

ARTICLE INFO

Keywords:
Fission track
(U-Th)/He
Zircon
Apatite
Carlin-type gold deposit
Southwestern Guizhou

ABSTRACT

The Dian-Qian-Gui area in southwestern China is the second-largest concentration of the Carlin-type gold deposits in the world, and the southwestern Guizhou is the most important gold-producing district of the Dian-Qian-Gui area. Dating of the Carlin-type gold deposits is always a challenge due to the lack of ore-stage minerals which are suitable for conventional radiometric dating. Low-temperature thermochronometers, including fission track and (U-Th)/He, are temperature-sensitive radiometric dating techniques and have been successfully applied to elucidate many aspects of ore deposits, including the timing and duration of mineralization processes.

In this study, zircon fission track, zircon (U-Th)/He and apatite fission track dating techniques were applied to the Carlin-type gold deposits in southwestern Guizhou. Samples for zircon and apatite analyses were collected from mineralized or altered sedimentary rocks in Shuiyindong, Taipingdong, Bojitian, Yata and Getang gold deposits. Four groups of thermochronological ages were obtained, i.e., 192–216 Ma, 132–160 Ma, 88 Ma, and 19–40 Ma, which are considered to be the records of four geological thermal events. Of them, most zircon fission track ages and all zircon (U-Th)/He ages concentrate in 132–160 Ma. Thermochronological constraints, combined with field relationships, suggest that the mineralization of the Carlin-type gold deposits in southwestern Guizhou most likely occurred in this period. Partial zircon fission track ages are in 192–216 Ma. They may record the cooling timing of a pre-ore thermal event caused by the Indosinian orogeny, which is supported by the paleogeotemperature restoration. A few zircon grains with high U content yield fission track age of 88 Ma, which may record a post-ore thermal event associated with the intrusion of local mafic dykes. All apatite fission track ages range in 19–40 Ma, which may record a lower temperature but extensive hydrothermal superimposition in the Cenozoic. Additionally, a corresponding relationship between zircon fission track ages and stratigraphic sequences was identified in the Huijiabao anticline, which is considered to reflect the decrease of temperature and duration of ore-forming hydrothermal activity from lower to upper stratigraphic sequences.

1. Introduction

The Carlin-type gold deposits, which are among the largest hydrothermal gold deposits in the world (Kesler et al., 2005), are mainly present in Nevada, USA and southwestern China (Tretbar et al., 2000; Hu et al., 2002; Arehart et al., 2003; Cline et al., 2005; Kesler et al., 2005; Su et al., 2008,2018; Muntean et al., 2011; Hu and Zhou 2012). The Dian-Qian-Gui area, located in the junction of the Yunnan, Guizhou and Guangxi provinces of southwestern China, is an important area for the Carlin-type gold deposits (Fig. 1 a, b; Cunningham et al., 1988; Ashley et al., 1991; Hu et al., 2002, 2015, 2017a, 2017b; Peters et al., 2007; Su et al., 2009a,2018) where more than 200 gold deposits or occurrences have been identified (Fig. 1b; Hu et al., 2007), making it the second-largest concentration of the Carlin-type gold deposits in the world (Hu et al., 2002, 2017b; Su et al., 2018). The southwestern Guizhou is the most important gold-producing district of the Dian-Qian-Gui area where many large (> 20 t Au) and super-large (> 100 t Au) gold deposits are hosted (e.g., Shuiyindong, Lannigou, Taipingdong, Zimudang, Getang and Yata; Fig. 1c) and over 1000 tons of gold reserves are expected to exploit (Liu et al., 2009).

Determining the mineralization ages of the Carlin-type gold deposits is integral to elucidate their links to associated geological events and to

* Corresponding author at: State Key Laboratory of Ore Deposit Geochemistry, Institute of Geochemistry, Chinese Academy of Sciences, Guiyang 550081, China.
E-mail address: huruizhong@vip.gyig.ac.cn (R. Hu).

https://doi.org/10.1016/j.oregeorev.2019.103178
Received 2 March 2019; Received in revised form 2 September 2019; Accepted 13 October 2019
Available online 15 October 2019
0169-1368/

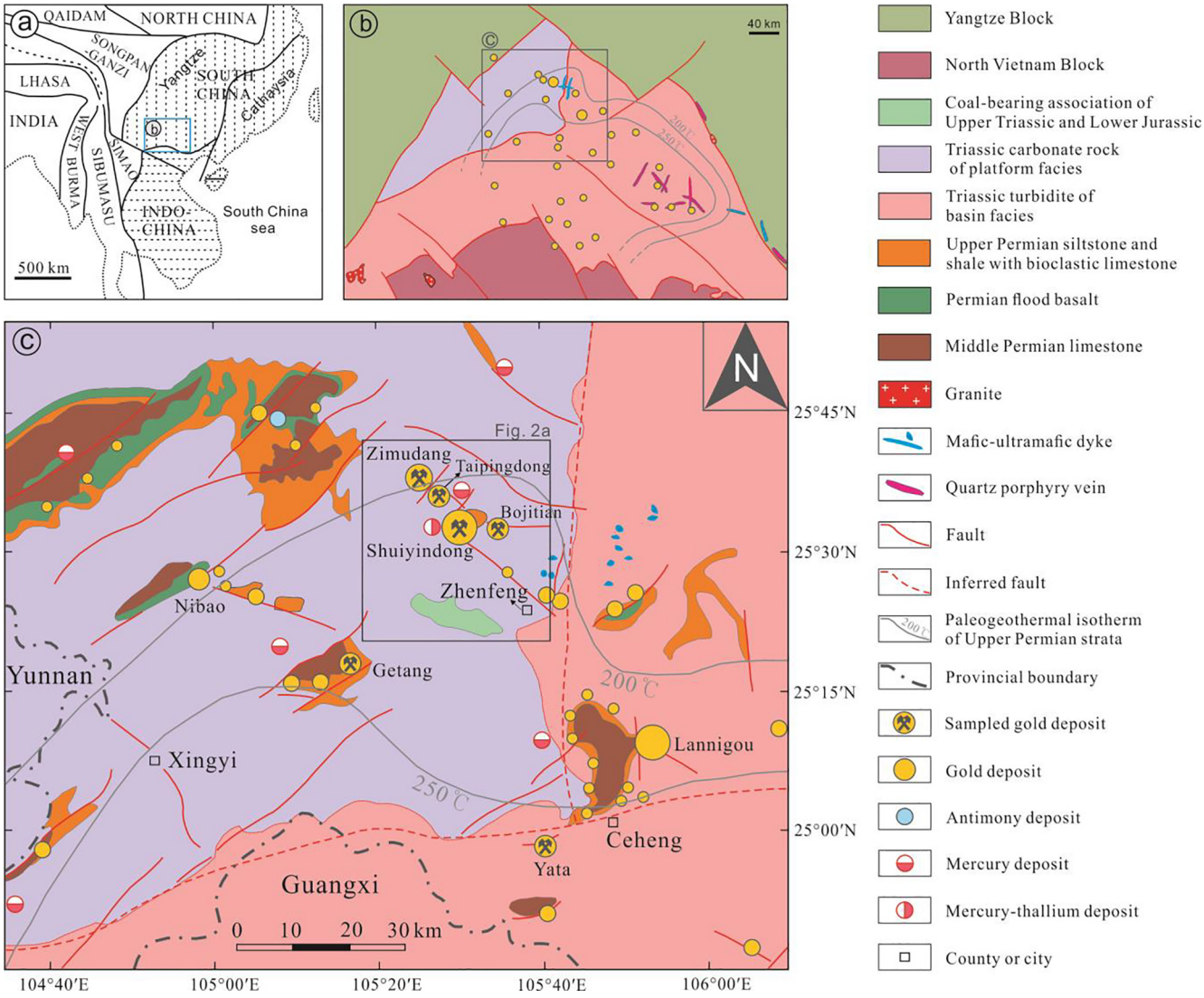

Fig. 1. (a) Sketch map of major tectonic units in southeastern Asia (modified from Cai and Zhang, 2009). (b) Simplified geologic map of the Dian-Qian-Gui area showing the distribution of the Carlin-type gold deposits in the Youjiang basin (modified from Chen et al., 2015). (c) Geologic map of southwestern Guizhou showing the locations of sampled Carlin-type gold deposits (modified from Zhang et al., 2003; Su et al., 2009a). The paleogeothermal isotherms were estimated from the vitrinite reflectance data by Zhuang (1995).

develop a suitable genetic model for these important deposits (Chakurian et al., 2003). However, dating of Carlin-type gold deposits is always a challenge as few suitable ore-stage minerals can be used for conventional radiometric dating. Moreover, the fine-grained characteristic of the ore-stage minerals makes them difficult to be separated or analyzed (Hofstra and Cline, 2000). In the past decades, although various radiometric methods have been used in an attempt to determine the ages of the Carlin-type gold deposits in southwestern Guizhou, conflicting data and equivocal interpretations were obtained, which require authentication by additional studies.

Low-temperature thermochronometers, including fission track and (U-Th)/He, are temperature-sensitive radiometric dating techniques and have many successful applications on hydrothermal ore deposits. For example, low-temperature thermochronology has been used to constrain the timing and duration of mineralization (Chakurian et al., 2003; McInnes et al., 2005), reconstruct the thermal evolution history of hydrothermal systems (McInnes et al., 2005; Betsi et al., 2012), map thermal halos associated with mineralization (Cunningham et al., 2004; Marton, 2015), calculate the exhumation rate and evaluate the preservation potential of ore deposits (Zhao et al., 2015; Liu et al., 2017). As we know, heat is a key factor that exerts a major control on fluid circulation and metal solubility for hydrothermal ore deposits (Marton et al., 2010). Heated ore-forming fluids flowing through rocks would leave a clear thermal “fingerprint” on their passage (Arehart and Donelick, 2006). So, an alternative way to determine the age of hydrothermal ore deposit is to date the relevant thermal event. Since the ore-forming temperature of Carlin-type gold deposit is generally higher than the closure temperature of fission track and (U-Th)/He system in zircon and apatite (see Section 5.1), low-temperature thermochronology can be used to estimate the absolute timing of the metallogenic thermal event and therefore constrain the mineralization age of the Carlin-type gold deposit (McInnes et al., 2005; Reiners et al., 2005). Actually, low-temperature thermochronology has already provided important constraints on the age of the Carlin-type gold mineralization in Nevada (Arehart et al., 1993, 2003; Hofstra et al., 1999; Chakurian et al., 2003; Cline et al., 2005) and some other hydrothermal ore deposits (Yuan et al., 2007, 2009, 2013; Deng et al., 2014; Wolff et al., 2015; Fu et al., 2019a,b). In this study, we applied zircon and apatite fission track and zircon (U-Th)/He dating to several representative Carlin-type gold deposits in southwestern Guizhou. The aim of this study is to constrain the mineralization age of these deposits, as well our low-temperature thermochronological data reveal multiple

geological thermal events in the region and record the behavior of hydrothermal evolution in the ore-forming process.

2. Geology setting

2.1. Regional geology

The Carlin-type gold deposits in the Dian-Qian-Gui area are restricted to the Youjiang basin, which is located in the southwestern margin of the South China Craton and adjacent to the Indochina Block to the south (Fig. 1a, b). The basin developed on the Lower Paleozoic basement and has experienced three distinctive stages, including rift basin during the late Early Devonian to Late Devonian, passive continental margin during the Early Carboniferous to Early Triassic, and foreland basin during the Middle Triassic (Du et al., 2013). Finally, the Youjiang basin was uplifted into land by the Indosinian orogeny at the end of the Late Triassic and subsequently folded by the Yanshanian orogeny after the Early Jurassic.

Southwestern Guizhou lies in the north part of the Youjiang basin (Fig. 1b). The Carlin-type gold deposits in this region are hosted chiefly in the Permian and Triassic sedimentary rocks (Zhang et al., 2003). From the northwest to the southeast of the basin, the sedimentary environment and related rock associations change from shallow-water platform facies carbonate and clastic rocks to deep-water basin facies turbidites (Fig. 1b, c; Zhang et al., 2003; Su et al., 2009a). The facies boundary is defined by the NEE-trending Nanpanjiang fault and an inferred NS-trending Puding-Ceyang fault (Fig. 1c; Zhang et al., 2003). The intensity of stratigraphic deformation caused by orogeny was variable in different facies. The platform facies rocks were gently folded or domed (Fig. 2), while the deep basin rocks were tightly folded resulting in high-angle reverse faults (Wang et al., 1995; Liu et al., 2002; Su et al., 2009a). In addition, a regional unconformity was generated by crustal uplift associated with the emplacement of the Emeishan plume at the end of the Middle Permian (He et al., 2003). The unconformity interface, which was termed as SBT (altered zone) by Chinese geologists (Fig. 3a, c), is generally considered as the migration channel for ore-forming hydrothermal fluids (Liu et al., 2002; Liu, et al., 2006; Su et al., 2009a; Chen et al., 2015). Corresponding to the above-mentioned three types of structures, the gold deposits in southwestern Guizhou are typically controlled by anticlines or domes (e.g., Shuiyindong, Taipingdong, and Bojitian deposits; Figs. 2a and 3a), high angle reverse faults (e.g., Yata and Lannigou deposits; Fig. 3b), and unconformity interface (e.g., Getang and Nibao deposits; Fig. 3c). No felsic igneous intrusions are present in the vicinity of the gold deposits in southwestern Guizhou, while some small mafic dykes crop out sporadically along the Puding-Ceyang fracture (Fig. 1c; Su et al., 2009a). These mafic dykes were emplaced in 84–88 Ma (Chen et al., 2009b; Liu et al., 2010) and well away from known gold deposits.

2.2. Deposit geology

The deposits in this study involve all three structure-controlled types of gold deposits mentioned above.

The Shuiyindong, Taipingdong and Bojitian deposits are located along the axis of the Huijiabao anticline (Fig. 2) and share similar geological characteristics. The Huijiabao anticline is an EW-trending symmetrical fold with a length of about 20 km, a width of about 6 km and dip angles of 5–20° on both limbs (Liu et al., 2006). The anticlinal axis inclines eastward (Fig. 2a) and displays an undulating shape. Four sets of faults cut the anticline (Fig. 2), including EW-trending reverse faults, NE and NS-trending normal faults, as well as interlayer faults (Xia, 2005; Peng et al., 2014). Sedimentary strata in the anticline include the Middle Permian to Triassic formations (Figs. 2 and 3a), which consist of bioclastic limestone, siltstone, and argillite (Su et al., 2008). Gold mineralization occurred mainly in impure limestone and calcareous siltstone of the Upper Permian Longtan Formation, which is about 300 m thick and can be divided into three units (Fig. 3a; Liu, 2001). A small number of gold orebodies are hosted in the Upper Permian Changxing Formation to the Lower Triassic Yelang Formation. In addition, some orebodies with lower gold but higher antimony and arsenic grades are hosted in silicified, brecciated argillite and limestone in the unconformity interface (SBT; Fig. 3a; Liu et al., 2006). Overall, orebodies in these deposits are chiefly present as stratiform, stratoid or lenticular which are in accordance with favorable lithology or the unconformity interface, and are gradually thinned away from the anticline axis (Fig. 3a; Peng et al., 2014).

The Yata deposit is controlled by high angle reverse faults (Fig. 3b). Gold mineralization is mainly hosted in the second unit of the Middle Triassic Xuman Formation, which is composed of turbidite sandstone, argillite, and argillaceous limestone (Fig. 3b; Ashley et al., 1991). More than 40 ore veins are confined within a narrow EW-trending zone and are controlled by reverse faults that cut the south limb of the EW-trending Huangchang anticline and subsidiary folds (Fig. 3b; Han et al., 1999).

The Getang deposit is located in the southeastern part of the core of the SE-NW-trending Getang dome (Zheng et al., 1989). The mineralization is mainly controlled by the unconformity interface (SBT; Fig. 3c). Gold deposited mainly in lenticular breccias, which are composed of silicified limestone, brecciated black shale and siliceous rock (Fig. 3c; Zhang et al., 2003). The thickness of the mineralized zone varies from 0.5 to 30 m (Zhang et al., 2003).

Despite the differences in structure and lithology, the Carlin-type gold deposits in southwestern Guizhou are similar in many aspects. Hydrothermal alteration generally consists of silicification, argillization, sulfidation and decarbonatization (Hu et al., 2002; Su et al., 2008). The hydrothermal mineral assemblages indicate that the deposits include a main stage of arsenian pyrite + arsenopyrite + marcasite + jasperoid quartz ± milky vein quartz + dolomite + clay minerals and a late stage of realgar ± orpiment ± stibnite ± cinnabar + calcite + euhedral quartz. Gold occurred primarily as invisible nanometer-sized inclusions or lattice gold in arsenian pyrite and arsenopyrite, with lesser amounts in realgar and clay minerals (Mao, 1991; Su et al., 2008; Peng et al., 2014). Visible micrometer-sized native gold was also locally identified (Zhang et al., 2005; Su et al., 2008). In addition, these deposits are characterized by similar ore-forming fluid features, including low temperatures (~120–270 °C), high pressures, low salinity, moderate acidity, low fO_2, and high CO_2 and H_2S concentration (Hu et al., 2002; Zhang et al., 2003; Su et al., 2009a; Gu et al., 2012; Chen et al., 2015). The similarities suggest that these Carlin-type gold deposits in southwestern Guizhou may be generated through a similar mechanism, or associated with the same geological processes.

3. Samples and analytical methods

3.1. Samples collecting and preparing

Samples for zircon and apatite analyses were collected from the Shuiyindong, Taipingdong, Bojitian, Yata and Getang gold deposits in southwestern Guizhou (Fig. 1c), and the detailed descriptions of samples including the location, elevation, stratigraphic sequence, lithology and alteration characteristics are outlined in Table 1. All samples are mineralized or altered sedimentary rocks, including impure bioclastic limestone, calcareous sandstone, siltstone and argillite, and the associated strata are the Upper Permian or Middle Triassic formations. Considering that the zircons and apatites in these rocks are mostly detrital in origin, the rocks with high terrigenous clastic content were preferentially collected. In addition, each sample is more than 10 kg in order to separate enough zircon and apatite grains. All samples were crushed, ground and sifted. Both zircon and apatite grains were separated using conventional heavy liquid and magnetic techniques and then handpicked under a binocular microscope. The temperature was

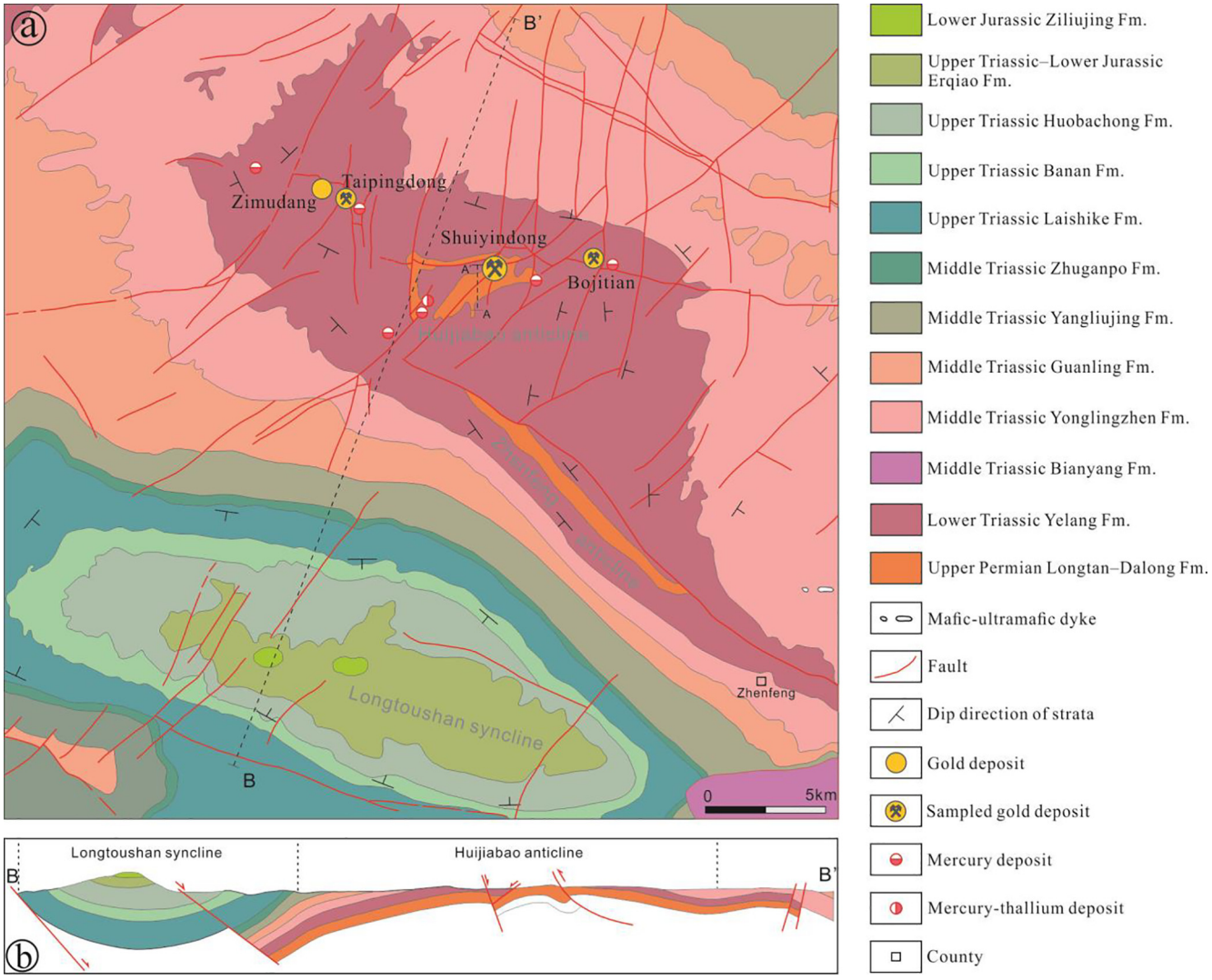

Fig. 2. (a) Geologic map of the Huijiabao anticline and the Longtoushan syncline (modified from Regional Geological Survey Team of Guizhou Geological Bureau, 1981; Guizhou Institute of Geological Survey, 2017). (b) Cross-section of the Huijiabao anticline and the Longtoushan syncline (modified from Chen et al., 2017). Abbreviations: Fm. = Formation.

kept below 80 °C during sample preparation to avoid fission tracks or helium being reset in minerals.

3.2. Zircon and apatite fission track analytical methods

The fission track analyses were performed in the Beijing Zekangen Technology Co., Ltd., and the external detector method was used. The zircon and apatite grains were mounted in FEP Teflon sheet and epoxy resin, respectively, and then they were ground and polished to expose internal grain surfaces. In order to reveal spontaneous tracks, zircon grains were etched about 25 h in NaOH/KOH (= 1:1) eutectic etchant at 210 °C and apatite grains were etched 30 s by 7% HNO_3 at 25 °C (Yuan et al., 2007). Thin low-uranium (< 4 ppb) muscovites as external detectors were firmly attached onto the etched zircon and apatite surfaces. All sample-detector pairs were irradiated in a well-thermalized (Cd for Au > 100) neutron flux in the 492 Swim Reactor in Beijing. Neutron fluence for zircon and apatite samples was respectively monitored using the CN2 and CN5 standard glass dosimeters (Bellemans et al., 1995), which were also covered by muscovite detectors. After irradiation, muscovite detectors were etched for 20 min in 40% HF at 25 °C to reveal induced tracks (Yuan et al., 2007). Both spontaneous and induced fission track counting was performed using a dry objective at 100 × 10 magnification. Only those grains with prismatic sections parallel to the c-crystallographic axis were analyzed (Gleadow et al., 1986; Green et al., 1986; Bernet and Garver, 2005). Fission track ages were calculated using the IUGS-recommended Zeta calibration method (Hurford and Green, 1982; Hurford, 1990), and errors were calculated using the conventional method of Green (1981). The central age is a weighted average age for all grains in a sample, while the pooled age sums together all grains' spontaneous and induced tracks within a sample to arrive at a single estimated age.

3.3. Zircon (U-Th)/He analytical method

Zircon (U-Th)/He analyses were performed in the Arizona Radiogenic Helium Dating Laboratory at the University of Arizona and followed the general procedures outlined in Reiners et al. (2004) and Reiners (2005). Zircon grains with euhedral crystals and a minimum radius of 60 μm, free of obvious fractures and inclusions were selected under microscope. The dimensions of individual grains were measured on digital photomicrographs to allow for later calculation of the alpha correction factor (Ft). Grains were packed individually in 1 mm Nb foil packets and then heated under a laser to extract ^{4}He. The released ^{4}He was spiked with ^{3}He for measurement by isotope dilution. Then the ^{4}He and ^{3}He were measured using a Blazers quadrupole mass spectrometer (QMS) with a Channeltron electron multiplier. The ^{4}He content of each

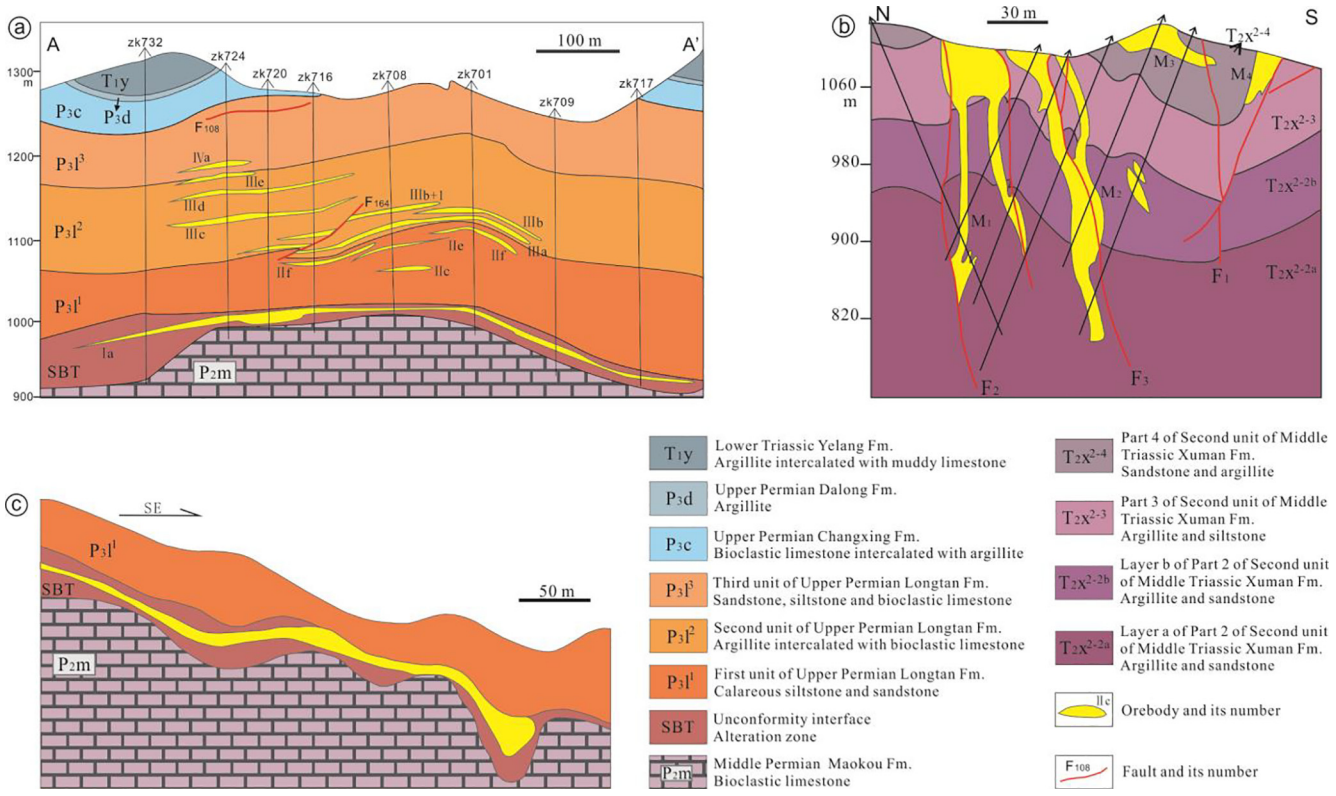

Fig. 3. Cross-sections showing mineralization of typical Carlin-type gold deposits in southwestern Guizhou. (a) Shuiyindong deposit (modified from Liu et al., 2006), the cross-section is along the A–A′ exploration line in Fig. 2a. (b) Yata deposit (modified from Zhang et al., 2003; Su et al., 2009a). (c) Getang deposit (modified from Wang et al., 1994). Abbreviations: Fm. = Formation.

grain was determined by comparing the sample $^{4}He/^{3}He$ ratio to the measured $^{4}He/^{3}He$ ratio of a known volume of reference ^{4}He gas standard. After He measurement, zircon-bearing foil packets were transferred to Teflon vials and spiked with calibrated solution of ^{233}U, ^{229}Th and ^{90}Zr. The zircons and Nb foil packets were then dissolved in high-pressure digestion vessels. Spiked sample solutions were analyzed for U, Th and Zr content by isotope dilution on a high-resolution (single-collector) Element-2 ICP-MS. The measured U, Th and ^{4}He content of individual grain was used to calculate a raw age, then alpha-ejection was corrected using the method described in Farley (2002) to obtain a corrected age.

4. Results

4.1. Zircon fission track ages

Twenty zircon samples from five gold deposits were analyzed, and the results are summarized in Table 2. Each sample contains 2–37 zircon grains. The fission track central ages of these zircon samples range from 120 to 202 Ma (Table 2). The χ^2 test was used to assess if a fission track grain age distribution is "overdispersed" relative to the expectation for count statistics for radioactive decay (Galbraith, 1981). Fifteen zircon samples have the $P(\chi^2) > 5\%$, which indicates that the grain ages from each of the 15 samples belong to a single population and display the characteristic of convergent age. In this case, the central age and pooled age are valid. For these samples, zircon central ages concentrate in two groups: the samples from the Shuiyindong, Bojitian, Yata and Getang deposits yield an age range of 120–177 Ma (typically concentrate in 135–156 Ma), while the samples from the Taipingdong deposit have an age range of 192–202 Ma (Fig. 4a).

Besides, five samples (SYD-6, SYD-7, BJT-1, TPD-7, YT-5) have the $P(\chi^2) < 5\%$, which indicates that the grain ages from each of the 5 samples do not belong to a single population and commonly represent a mixed age distribution (Brandon, 2002). The central age and pooled age are clearly not appropriate for mixed distributions (Green, 1981; Galbraith and Laslett, 1993). A better approach is to decompose the fission track grain age distribution into a set of component distributions and to interpret the fission track results using the average grain ages for those components (Brandon, 2002). Therefore, the BINOMFIT program (Brandon, 2002) with the binomial peak-fitting method (Galbraith and Green, 1990; Galbraith and Laslett, 1993) was used to decompose fission track grain ages of the 5 samples. As the result shown in Table 3 and Fig. 4b, it is apparent that: (1) Each of the 5 samples can be decomposed into two age components. Of them, four samples (SYD-6, SYD-7, BJT-1 and YT-5) yield younger age components with a range of 126–153 Ma and older age components with a range of 201–216 Ma. One sample (TPD-7) yields a younger age component of 88 Ma and an older age component of 135 Ma. (2) For each of the 5 samples, the ages of different components display a negative correlation with their U content. i.e., the component with older age has lower average U content, while the component with younger age has higher average U content. The component in TPD-7 sample with the youngest age (88 Ma) has the highest average U content.

By comparison, the decomposed component ages (126–153 Ma and 201–216 Ma) of the SYD-6, SYD-7, BJT-1 and YT-5 samples are broadly consistent with the convergent ages (135–156 Ma and 192–202 Ma) of the samples with $P(\chi^2) > 5\%$ (Fig. 4a, b). The older component age of the TPD-7 sample (135 Ma) is also consistent with the younger convergent ages (135–156 Ma) of the samples with $P(\chi^2) > 5\%$ (Fig. 4a, b). The histogram of the combined zircon fission track data of convergent ages and decomposed component ages shows two main groups of ages: 192–216 Ma and 135–156 Ma (Fig. 4c).

4.2. Apatite fission track ages

Seven apatite samples from three gold deposits were analyzed, and

Table 1
A summary of sample location, elevation, stratigraphic sequence, lithology and alteration characteristics.

Deposit	Sample	Lithology	Mineralization and alteration	Elevation	Strata	Sampling location
Shuiyindong	SYD-5	Bioclastic limestone	Silicification, with hydrothermal pyrite and arsenopyrite, about 5 g/t Au	1240m	Middle of P_3l^2	North downhill in line 15, IIIb + 1 orebody
	SYD-6	Argillite intercalated with limestone	With hydrothermal pyrite	1240m	Middle of P_3l^2	North downhill in line 15, floor wall rock adjacent to IIIb + 1 orebody
	SYD-7	Argillite intercalated with limestone	Weak silicification, with hydrothermal pyrite and arsenopyrite	1240m	Middle of P_3l^2	Line 0, roof wall rock adjacent to IIIc orebody
	SYD-8	Bioclastic limestone	Silicification, with hydrothermal pyrite and arsenopyrite	–	P_3l	Ore heap samples
	SYD-9	Sandy limestone	With hydrothermal pyrite and arsenopyrite	–	P_3l	Ore heap samples
	SYD-11	Argillite intercalated with limestone	With hydrothermal pyrite and arsenopyrite	–	P_3l	Ore heap samples
	SYD-12	Bioclastic limestone	Silicification, with hydrothermal pyrite	–	P_3l	Ore heap samples
	SYD-13	Bioclastic limestone	Silicification, with hydrothermal pyrite and arsenopyrite	–	P_3l	Ore heap samples
	SYD-14	Calcareous siltstone	–	–	P_3l	Ore heap samples
	SYD2-5	Bioclastic limestone	Silicification, with hydrothermal pyrite, native gold, about 2 g/t Au	1210m	Middle of P_3l^2	Uphill in line 5, IIIb orebody
	SYD2-8	Bioclastic limestone	Silicification, with hydrothermal pyrite, about 100 g/t Au	1170m	Bottom of P_3l^2	South of line 25, IIIa orebody, near F_{163} fault
	SYD2-9	Bioclastic limestone	Silicification, with hydrothermal pyrite and arsenopyrite	1150m	Bottom of P_3l^2	Downhill in line 23, IIIa orebody
Bojitian	BJT-1	Sandy limestone	Silicification, argillization	570m	Upper part of P_3l^2	700 m depth of drill hole ZK26341, wall rock adjacent to orebody
	BJT-2	Sandy limestone	Silicification, carbonatization	503m	Bottom of P_3l^2	767 m depth of drill hole ZK26341, wall rock adjacent to orebody
Taipingdong	TPD-7	Bioclastic limestone	Silicification, with hydrothermal pyrite, about 2–3 g/t Au	1272m	Middle of P_3l^3	East mining area, Line 16 transverse drift, 520S, IVb orebody
	TPD-8	Bioclastic limestone	Silicification, with hydrothermal pyrite, about 10 g/t Au	1272m	Lower part of P_3l^3	East mining area, Line 16 transverse drift, 520S-2 uphill, IVa orebody
	TPD-9	Argillite intercalated with limestone	With hydrothermal pyrite	1272m	Middle of P_3l^3	East mining area, Line 8 transverse drift, 504 N, floor wall rock adjacent to IVb orebody
	TPD-10	Sandy bioclastic limestone	Silicification, with hydrothermal pyrite and arsenopyrite	1302m	Middle of P_3l^3	East mining area, 404 ore drift, IVb orebody
	TPD-15	Sandy bioclastic limestone	Silicification, with hydrothermal pyrite and arsenopyrite, 5.48 g/t Au	1302m	Middle of P_3l^3	East mining area, 404 IVb + 1 ore drift
	TPD-19	Bioclastic limestone	Silicification, with hydrothermal pyrite, 6.08 g/t Au	1272m	Middle of P_3l^3	East mining area, 504 IVb + 1 ore drift
Yata	YT-5	Calcareous sandstone	Silicification, with hydrothermal pyrite and arsenopyrite	979m	T_2x	Orebody inIopencast stope, N24°54′49.76″, E105°39′06.81″
	YT-7	Calcareous siltstone	Silicification, with hydrothermal pyrite and arsenopyrite	979m	T_2x	Orebody inIopencast stope, N24°54′49.76″, E105°39′06.81″, 30 m east to YT-5
	YT-8	Calcareous siltstone	With hydrothermal pyrite and arsenopyrite	1021m	T_2x	Orebody inIopencast stope, N24°54′47.50″, E105°39′11.77″
	YT-12	Calcareous sandstone	Silicification, with hydrothermal pyrite and realgar, 1.54 g/t Au	990m	T_2x	Orebody inIopencast stope, N24°54′47.66″, E105°39′15.49″, Line 36
	YT-13	Calcareous sandstone	Silicification, with hydrothermal pyrite, 0.50 g/t Au	993m	T_2x	Orebody inIopencast stope, N24°54′48.84″, E105°39′18.74″
Getang	GT-2	Bioclastic limestone	Silicification, with hydrothermal pyrite	1290m	P_3l^1	No.13 primary ore body

Notes: P_3l, P_3l^1, P_3l^2 and P_3l^3 represent the Upper Permian Longtan formation and its first, second and third units, respectively. T_2x represents the Middle Triassic Xuman formation.

Table 2
Zircon and apatite fission track analytical results for samples from 5 gold deposits in southwestern Guizhou.

Sample	No. of grains	Spontaneous track		Induced track		Dosimeter glass		$P(\chi^2)$(%)	Central age (Ma) (± 1σ)	Pooled age (Ma) (± 1σ)	Average U content (ppm)
		N_s	$\rho_s(10^5/cm^2)$	N_i	$\rho_i(10^5/cm^2)$	N_d	$\rho_d(10^5/cm^2)$				
Zircon											
SYD-5	7	996	168.871	591	100.203	10,030	14.051	75.9	120 ± 8	120 ± 8	276.03
SYD-6	13	2126	155.595	914	66.893	10,030	14.28	0	167 ± 14	167 ± 9	177.24
SYD-7	26	4471	93.395	2035	42.509	10,030	14.624	0.6	163 ± 9	162 ± 8	107.55
SYD-8	19	2922	92.602	1418	44.938	10,030	14.967	20.1	156 ± 8	156 ± 8	107.78
SYD-9	25	5611	119.665	2555	54.49	10,030	15.197	9.3	167 ± 8	168 ± 8	134.09
SYD-11	13	1384	83.31	751	42.206	10,030	15.426	97.9	144 ± 9	144 ± 9	112.67
SYD-13	11	1755	139.481	919	73.039	10,030	15.655	23.4	150 ± 9	151 ± 9	170.59
SYD-14	26	6435	106.099	2913	48.029	10,030	15.884	87.3	177 ± 8	177 ± 8	111.38
SYD2-8	37	4137	139.356	1373	46.25	8055	10.587	32.9	143 ± 7	143 ± 7	163.47
SYD2-9	36	7491	135.356	2771	50.07	8055	11.077	8.9	135 ± 6	135 ± 5	167.48
BJT-1	31	3924	136.708	1541	53.687	7846	13.263	1.9	162 ± 9	162 ± 8	148.22
BJT-2	35	5943	95.059	2606	41.683	7846	14.097	85.0	154 ± 7	154 ± 7	108.69
TPD-7	12	1363	171.182	642	80.63	8055	12.424	0.5	115 ± 9	119 ± 7	254.11
TPD-8	4	606	166.616	243	66.811	7846	16.877	22.5	202 ± 18	201 ± 17	153.09
TPD-9	20	3113	134.188	1357	58.494	7846	17.294	7.8	192 ± 11	189 ± 10	127.88
TPD-10	28	4133	142.043	1227	42.2	7846	12.012	56.8	193 ± 10	193 ± 10	128.44
GT-2	2	262	85.978	1136	44.63	7846	15.209	42.5	140 ± 16	140 ± 16	101.97
YT-5	21	2963	200.949	1018	69.04	8055	11.567	0	152 ± 10	151 ± 7	222.65
YT-7	17	2280	164.499	1036	74.746	7846	14.792	56.1	156 ± 8	156 ± 8	192.07
YT-8	13	1854	235.758	720	91.556	8055	12.057	27.6	139 ± 8	140 ± 8	272.17
Apatite											
SYD-7	6	31	0.623	304	6.112	8116	17.859	99.1	36 ± 7	36 ± 7	4.17
SYD-12	35	757	4.975	5256	34.541	7978	11.792	99.7	35 ± 2	35 ± 2	35.07
SYD2-5	29	137	0.814	1248	7.416	5782	13.552	97.3	30 ± 3	30 ± 3	7.38
TPD-8	14	35	0.64	362	6.623	5782	11.782	29.2	25 ± 5	23 ± 4	6.11
TPD-9	18	49	0.578	432	5.092	5782	17.294	99.5	40 ± 6	40 ± 6	4.06
TPD-10	33	130	0.427	1433	4.704	5782	12.012	62.1	22 ± 2	22 ± 2	5.19
GT-2	10	16	0.105	599	3.924	5782	10.011	34.9	19 ± 5	19 ± 5	1.83

Notes: SYD, BJT, TPD, YT and GT represent Shuiyindong, Bojitian, Taipingdong, Yata and Getang gold deposits, respectively. ρ_s = Density of spontaneous tracks on the internal surfaces of mineral grains analyzed. N_s = Total number of fission tracks counted in ρ_s. ρ_i = Density of induced tracks in the muscovite external detector for mineral grains analyzed. N_i = Total number of fission tracks counted in ρ_i. ρ_d = Density of induced tracks in muscovite external detectors over CN2 or CN5 dosimeter glass. N_d = Total number of fission tracks counted in ρ_d. $P(\chi^2)$ = χ^2 probability that all single-grain ages represent a single population of ages.

the results are summarized in Table 2. Each sample contains 6–35 apatite grains. The fission track central ages of apatite samples are concentrated in the range of 19–40 Ma (Table 2; Fig. 4d). All samples have the $P(\chi^2) > 5\%$, indicating that the grain ages from each sample should represent a single population, and thus the central age and pooled age are valid.

4.3. Zircon (U-Th)/He ages

Four samples from the Taipingdong and Yata deposits were analyzed, and the results are shown in Table 4 and Fig. 4e. Each sample contains 5 zircon grains. Quantile-Quantile plot was used to assess if grain ages from each sample belong to a normally distributed population (Wilk and Gnanadesikan, 1968). The correlation coefficients for the plots vary in the range of 0.92–0.99, indicating the grain ages from each sample follow a normal distribution pattern. Then Chauvenet's criterion was applied to detect if there are outliers in (U-Th)/He grain ages for each sample (Long and Rippeteau, 1974; Fitzgerald et al., 2006; Liu et al., 2017). The idea of the criterion is that all grain ages from a normally distributed population should lie within a probability of 1–1/(2n) (n is the grain number) centering on the mean, and those grain ages falling outside this range can be discarded. The test results suggest that there is no outlier in each of the 4 samples. In this case, the weighted average age of 5 grains in each sample was calculated by *Isoplot 4.15* to represent the true (U-Th)/He age of the sample. Therefore, the (U-Th)/He ages of the two samples from the Taipingdong gold deposit are 144.55 ± 12.53 Ma (2σ) and 160.21 ± 2.00 Ma (2σ), while the (U-Th)/He ages of the two samples from the Yata gold deposit are 132.23 ± 10.31 Ma (2σ) and 133.11 ± 14.34 Ma (2σ; Table 4; Fig. 4e). It is apparent that the (U-Th)/He age range of 132–160 Ma is consistent with the main zircon fission track age group of 135–156 Ma (Fig. 4c, e).

5. Interpretation and discussion

5.1. Low-temperature thermochronological records of multiple geological thermal events in southwestern Guizhou

As described above, all samples for low-temperature thermochronological dating were collected from the Upper Permian and Middle Triassic strata (Table 1). It is apparent that all zircon fission track ages are much younger than the formation ages of the corresponding strata, which indicates that the zircon fission track systems in these samples were subjected to thermal reset after the formation of the strata. The two groups of fission track central ages of zircon samples with $P(\chi^2) > 5\%$, i.e., 192–202 Ma and 135–156 Ma, probably record the cooling ages of two periods of geological thermal events later than the stratigraphic deposition.

However, for the samples SYD-6, SYD-7, BJT-1, YT-5 and TPD-7 with the $P(\chi^2) < 5\%$, each of them contains one older (~210 Ma in SYD-6, SYD-7, BJT-1 and YT-5, or 135 Ma in TPD-7) and one younger (~140 Ma in SYD-6, SYD-7, BJT-1 and YT-5, or 88 Ma in TPD-7) zircon fission track age components. These component ages should result from the differential annealing of zircons. In typical geological settings, zircon has an effective closure temperature of about 240 ± 30 °C (Brandon et al., 1998), but this estimate is sensitive to radiation damage in the zircon (Rahn et al., 2004). High radiation damage lowers the closure temperature, and in some cases, tracks in zircon may be annealed and the grain reset at temperatures of ca. 200 °C or less (Garver et al., 2002,2005). High U content is one of the main factors causing high radiation damage of zircon (Rahn et al., 2004; Garver et al., 2005). The above five samples all show a negative correlation between the

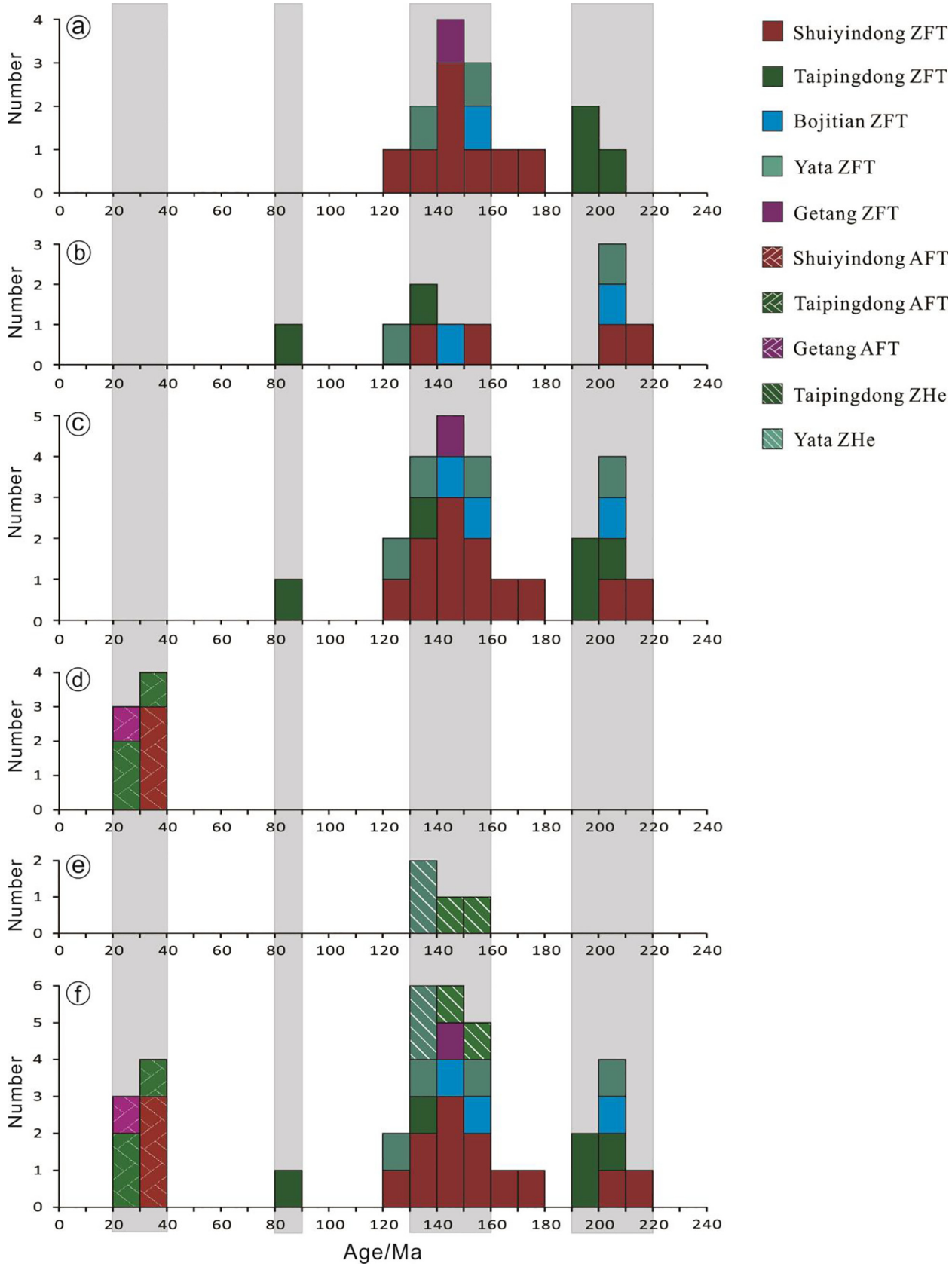

Fig. 4. Histogram of zircon fission track (ZFT), apatite fission track (AFT) and zircon (U-Th)/He (ZHe) ages obtained from five gold deposits in southwestern Guizhou. (a) The fission track central ages of 15 zircon samples with P(χ^2) > 5%. (b) The decomposed fission track component ages of 5 zircon samples with P (χ^2) < 5%. (c) The combination of figure a and b. (d) The fission track central ages of 7 apatite samples. (e) The (U-Th)/He ages of 4 zircon samples. (f) The combination of figure c, d and e. Four groups of low-temperature thermochronological ages can be identified from these histograms, i.e., 192–216 Ma, 132–160 Ma, 88 Ma and 19–40 Ma.

Table 3
Fission track component ages and average U content of decomposed component distributions of zircon grains from samples with P(χ^2) < 5%.

Sample	Central age (Ma) (± 1σ)	Component age (Ma)		Average U content (ppm)	
		Component 1	Component 2	Component 1	Component 2
SYD-6	167 ± 14	135	216	203	135
SYD-7	163 ± 9	153	204	115	88
BJT-1	162 ± 9	149	202	157	122
TPD-7	115 ± 9	88	135	275	244
YT-5	152 ± 10	126	201	253	182

Note: component decomposing and peak fitting were implemented by the BINOMFIT program.

component ages and the average U content of zircons in the components (Table 3). Therefore, it is presumed that two groups of zircons with different degrees of radiation damage may exist in each sample. When affected by a relatively low temperature thermal event, the tracks in zircons with high radiation damage were reset and record the cooling age of the thermal event, while the tracks in zircons with low radiation damage cannot be reset and still record the cooling age of an earlier thermal event. Therefore, two groups of zircons in the same sample may record the cooling ages of two different geological thermal events. This phenomenon has been confirmed in several previous studies (Seward and Rhoades, 1986; Carter, 1990; Laubacher and Naeser, 1994; Garver et al., 2005). In addition, the main two groups of decomposed component ages of the 5 samples are consistent with the two groups of convergent ages of the 15 samples with P(χ^2) > 5% (Fig. 4a, b), which also supports this assumption. The youngest zircon fission track age (88 Ma) was obtained from a zircon component in the TPD-7 sample. This age may have resulted from the abnormally high U content in the zircons (Table 3), which resulted in very high radiation damage and thus low closure temperature. Then these zircons were reset by a younger (88 Ma) thermal event at lower temperature. Based on the above analysis, the decomposed component ages of 201–216 Ma, 126–153 Ma and 88 Ma obtained from the five samples may record the cooling ages of three separate geological thermal events in this area.

Four samples from the Taipingdong and Yata deposits yield similar zircon (U-Th)/He ages of 132–160 Ma, which are much younger than the formation ages of the host strata. This indicates that a geological thermal event may have reset the (U-Th)/He system in zircons of these samples during 132–160 Ma. The zircon (U-Th)/He ages coincide with the younger group of zircon fission track ages (135–156 Ma; Fig. 4c, e), which further indicates the presence of a thermal event during this period.

The apatite fission track ages of all samples have P(χ^2) > 5% and are relatively concentrated (19–40 Ma; Fig. 4d). They may record the cooling age of a thermal event in the Cenozoic.

In summary, four groups of low-temperature thermochronological ages were obtained (Fig. 4f), i.e., 192–216 Ma, 132–160 Ma, 88 Ma and 19–40 Ma. The four groups of ages are probably the records of four geological thermal events in southwestern Guizhou.

5.2. Low-temperature thermochronological constraints on mineralization age of the Carlin-type gold deposits in southwestern Guizhou

Hydrothermal deposit is the product of geological thermal event. The ore-formation temperature of the Carlin-type gold deposits in southwestern Guizhou mainly ranges from 120 to 270 °C (Su et al., 2009a; Gu et al., 2012). The samples analyzed in this study were collected from orebodies or altered host rocks. Therefore, the fission track system in zircon (with closure temperature 240 ± 30 °C; Brandon et al., 1998), the (U-Th)/He system in zircon (with closure temperature 170–190 °C; Reiners, 2005) and the fission track system in apatite (with closure temperature 90–120 °C; Ketcham et al., 1999) in the samples can be reset during gold mineralization so that they can record the cooling age of the metallogenic thermal event of the Carlin-type gold deposits. In this case, the thermal events recorded by the three low-temperature thermochronometers should include the metallogenic thermal event. In other words, the metallogenic thermal event may

Table 4
(U-Th)/He analytical results for samples from two gold deposits in southwestern Guizhou.

Sample (Au grade)	No.	U/ng	1σ/%	Th/ng	1σ/%	He/pmol	1σ/%	Raw age/Ma	1σ/Ma	Spherical radius/μm	Ft	Corrected age/Ma	1σ/Ma	Weighted average age/Ma	2σ/Ma
TPD-15 (5.48 g/t)	1	0.5742	1.46	0.3936	1.43	0.3485	0.55	96.14	1.30	45.57	0.73	131.11	1.79	144.55	12.53
	2	1.0860	1.44	0.6969	1.44	0.7349	0.49	108.05	1.43	42.78	0.72	150.48	2.01		
	3	1.9111	1.47	1.4132	1.42	1.3050	0.48	106.91	1.41	46.33	0.74	145.03	1.94		
	4	0.7945	1.44	0.5827	1.43	0.5291	0.51	104.41	1.37	46.56	0.74	141.41	1.87		
	5	0.5854	1.44	1.0335	1.43	0.5108	0.53	113.21	1.36	44.12	0.72	157.29	1.90		
TPD-19 (6.08 g/t)	1	2.5058	1.44	0.7746	1.43	1.7916	0.38	122.36	1.66	49.89	0.76	161.50	2.21	160.21	2.00
	2	0.9635	1.43	0.2807	1.43	0.6719	0.45	119.84	1.66	45.50	0.74	162.77	2.27		
	3	1.2413	1.43	0.5194	1.42	0.8876	0.37	119.53	1.59	50.94	0.76	156.98	2.10		
	4	1.2875	1.43	0.6601	1.43	0.9685	0.45	123.21	1.64	54.42	0.78	158.96	2.13		
	5	0.9765	1.47	0.3150	1.44	0.6497	0.76	113.61	1.75	39.90	0.70	161.77	2.51		
YT-12 (1.54 g/t)	1	0.6207	1.45	0.5215	1.45	0.3858	0.75	95.47	1.35	39.54	0.70	137.28	1.97	132.23	10.31
	2	0.8756	1.44	0.0871	1.49	0.4890	0.39	100.39	1.43	39.73	0.70	142.84	2.05		
	3	0.2657	1.49	0.1373	1.44	0.1383	0.40	85.48	1.16	37.71	0.68	124.90	1.71		
	4	0.6840	1.44	0.1628	1.44	0.3411	1.89	86.99	2.02	37.87	0.69	126.44	2.94		
	5	2.7373	1.44	1.9981	1.43	1.5375	1.89	88.24	1.99	39.55	0.70	126.76	2.87		
YT-13 (0.50 g/t)	1	1.1763	1.45	0.6785	1.45	0.7853	1.81	108.03	2.39	51.97	0.76	141.30	3.14	133.11	14.34
	2	1.2695	1.42	0.7203	1.51	0.7194	1.81	92.01	2.02	56.05	0.78	117.91	2.60		
	3	2.3055	1.45	0.9071	1.51	1.4275	1.81	104.20	2.33	58.21	0.79	132.04	2.97		
	4	0.8749	1.56	0.4260	1.52	0.4846	1.81	91.46	2.09	46.94	0.74	123.32	2.83		
	5	2.1131	1.50	1.2777	1.56	1.4170	0.31	107.90	1.43	49.39	0.75	143.28	1.92		

Notes: TPD and YT represent Taipingdong and Yata gold deposits, respectively. Ft is a geometric correction factor for alpha ejection. The weighted average age of each sample was calculated by *Isoplot 4.15*.

occur in one or more periods of 192–216 Ma, 135–156 Ma, 88 Ma and 19–40 Ma.

Since the zircon (U-Th)/He ages range from 132 to 160 Ma, and most zircon fission track ages are concentrated in the range of 135–156 Ma, indicating that the zircon (U-Th)/He system and zircon fission track system have not been disturbed by thermal events with ages younger than 132 Ma (except for a small number of abnormally high U grains in TPD-7). This means that no thermal event has occurred after 132 Ma with a temperature higher than 170–190 °C (closure temperature of the zircon (U-Th)/He system), so the age of gold mineralization (with temperature up to 270 °C) would not be younger than 132 Ma. That is to say, it is unlikely that the gold mineralization occurred at 88 Ma and 19–40 Ma, and it could occur only at 192–216 Ma or 132–160 Ma.

Field relationships show that the Carlin-type gold deposits in the Huijiabao area are structurally controlled by the Huijiabao anticline (e.g., Shuiyindong, Taipingdong and Bojitian deposits; Fig. 2a and 3a) or faults that cut through the anticline (e.g., Zimudang deposit). The Huijiabao anticline is adjacent and parallel to the Longtoushan syncline (Fig. 2), and they were formed under the same stress. It is worth noting that some Lower Jurassic strata were found in the core of the Longtoushan syncline (Fig. 2; Wang, 1997), and these Jurassic strata were conformable to and folded together with the Upper Triassic strata (Fig. 2b; Guizhou Institute of Geological Survey, 2017). This field relationship indicates that the folds (including the Huijiabao anticline and Longtoushan syncline) and faults that cut the folds should form later than the Early Jurassic (Su et al., 2018). Therefore, the age of gold mineralization in the Huijiabao anticline (also southwestern Guizhou) should be younger than the Early Jurassic, which means that the mineralization most likely occurred at 132–160 Ma.

Over the past decades, a variety of conventional geochronological methods have been used to date the Carlin-type gold deposits in southwestern Guizhou, including Re-Os dating of pyrite and arsenopyrite (Chen et al., 2007,2015), Ar-Ar dating of sericite (Chen et al., 2009a), Sm-Nd dating of calcite (Su et al., 2009b; Wang, 2013), and Th-Pb dating of apatite (Chen et al., 2019). The pyrite and arsenopyrite Re-Os and sericite Ar-Ar ages of 193–235 Ma (Chen et al., 2007,2009a,2015) seem to be consistent with the older group of zircon fission track ages in this study. However, both pre-ore and ore-stage pyrites are present in gold ores, and it is very difficult to separate them because of their fine-grained nature and complex internal texture. The arsenopyrites are also fine-grained and have similar physical properties with pyrites, which makes them difficult to be separated from pre-ore pyrites. Additionally, the low Re and Os contents of the pyrite and arsenopyrite in these deposits result in large analytical uncertainty, which means that the age data are unreliable (Chen et al., 2019). Similarly, hydrothermal sericites are also easy to mix with detrital or authigenic micas from sedimentary rocks due to their extremely small size. Besides, the reported Ar-Ar age spectrum of the sericite is highly irregular and with no plateau, indicating the age is not reliable (Su et al., 2018). Therefore, the ages of pyrite, arsenopyrite and sericite are probably questionable. In contrast, the calcites intergrown with realgar are clearly the products of metallogenic stage (Su et al., 2009b), and the coarse calcite veins make it easy to separate pure calcites for dating. The apatites intergrown with hydrothermal quartz and auriferous pyrite are also of obvious hydrothermal origin and coeval with gold mineralization (Chen et al., 2019), and in situ analytical techniques can avoid the interference of detrital apatites in host rocks. Therefore, the ages of calcites and apatites may represent the true age of gold mineralization. The age range obtained by calcite Sm-Nd method and apatite Th-Pb method is 134–148 Ma (Su et al., 2009b; Wang, 2013; Chen et al., 2019), which is in agreement with the mineralization age of 132–160 Ma constrained by low-temperature thermochronology in this study, suggesting that the gold mineralization in southwestern Guizhou may indeed have occurred in this period.

5.3. Low-temperature thermochronology records the tectonic thermal event in southwestern Guizhou caused by the Indosinian orogeny

During the Middle Triassic, the collision between the Indosinian plate and the South China plate (Indosinian orogeny) transformed the Youjiang basin into a foreland basin (Du et al., 2013). At this time, voluminous detrital materials from the southwestern and southeastern margins were imported into the basin to form the thick Middle Triassic turbidite (Yang et al., 2012). Burial heating, tectonic heating and possible magmatic thermal activity heated the lower strata of the basin (Zhuang, 1995). Regional-scale vitrinite reflectance data (Zhuang, 1995) and conodont colour alteration index (CAI) data (Zhou, 1990) show that the highest paleogeotemperature experienced by the Upper Permian and Lower Triassic strata in southwestern Guizhou was higher than 200–250 °C. The paleogeothermal isotherms estimated from the vitrinite reflectance data (Fig. 1b, c) are also consistent with the conodont CAI isolines (Zhou, 1990; Zhuang, 1995). Based mainly on the illite crystallinity data, Suo et al. (1998) proposed that the Triassic strata in the Youjiang basin have undergone very low-grade metamorphism with temperature of 150–350 °C. Besides, a positive correlation between the highest paleotemperature and the thickness of overlying strata was identified by Zhou (1990), Zhuang (1995) and Suo et al. (1998), which indicates that burial heating is an important reason for paleogeotemperature increase.

At the end of the Late Triassic, the further development of the Indosinian orogeny made the Youjiang Basin uplift into land, which terminated the marine sedimentation of the basin and initiated its continental sedimentation and denudation process. According to basin filling characteristics and tectonic activities, Zhuang (1995) speculated that the duration of the highest temperature experienced by the Upper Permian strata was about 27 Myr. The above analysis indicates that the fission track system of zircon from the lower strata (e.g., the Upper Permian strata) of the Youjiang basin can be reset by the paleogeothermal temperature and duration during the Indosinian orogeny. Therefore, the oldest group of zircon fission track ages (192–216 Ma) obtained in this study may record the cooling age of the pre-ore thermal event in southwestern Guizhou caused by the Indosinian orogeny.

Besides, it is speculated that the Indosinian orogeny thermal event also occurred in the southern margin of the Youjiang basin, because it is closer to the collision boundary between the South China plate and the Indosinian plate (Fig. 1a, b). This thermal event may have driven the fluid circulation to form diabase-hosted gold deposits in the southern margin of the basin (e.g., Zhesang, Anna and Laozhaiwan deposits in southeastern Yunnan), as the timing of this thermal event is consistent with the mineralization age of these deposits (~215 Ma) obtained from rutile U-Pb, sericite Ar-Ar and gold-bearing sulfides Rb-Sr dating (Pi et al., 2016, 2017; Hu et al., 2017b; Su et al., 2018).

5.4. The spatial distribution of zircon fission track ages and the hydrothermal evolution in the Huijiabao anticline

Fig. 5a shows age-elevation plot of zircon fission track central ages of samples with exact sampling locations from three gold deposits hosted in the Huijiabao anticline. The average U content of zircons in Huijiabao anticline generally varies from 108 ppm to 177 ppm, while that of SYD-5 and TPD-7 samples is up to 276 ppm and 254 ppm, respectively (Table 2). The high U content makes the two samples obtain younger fission track ages than the other samples. If the two samples are removed from the age-elevation figure, the ages of the 7 samples from the Shuiyindong and Taipingdong deposits and the ages of the 2 samples from the Bojitian deposit will increase separately with elevation (Fig. 5a). The interpretation for this trend cannot be that the samples from different elevations successively passed the closure isotherm (or depth) of zircon fission track in the process of uplift and exhumation. The reasons include: (1) For the 7 samples from the Shuiyindong and Taipingdong deposits, the maximum elevation

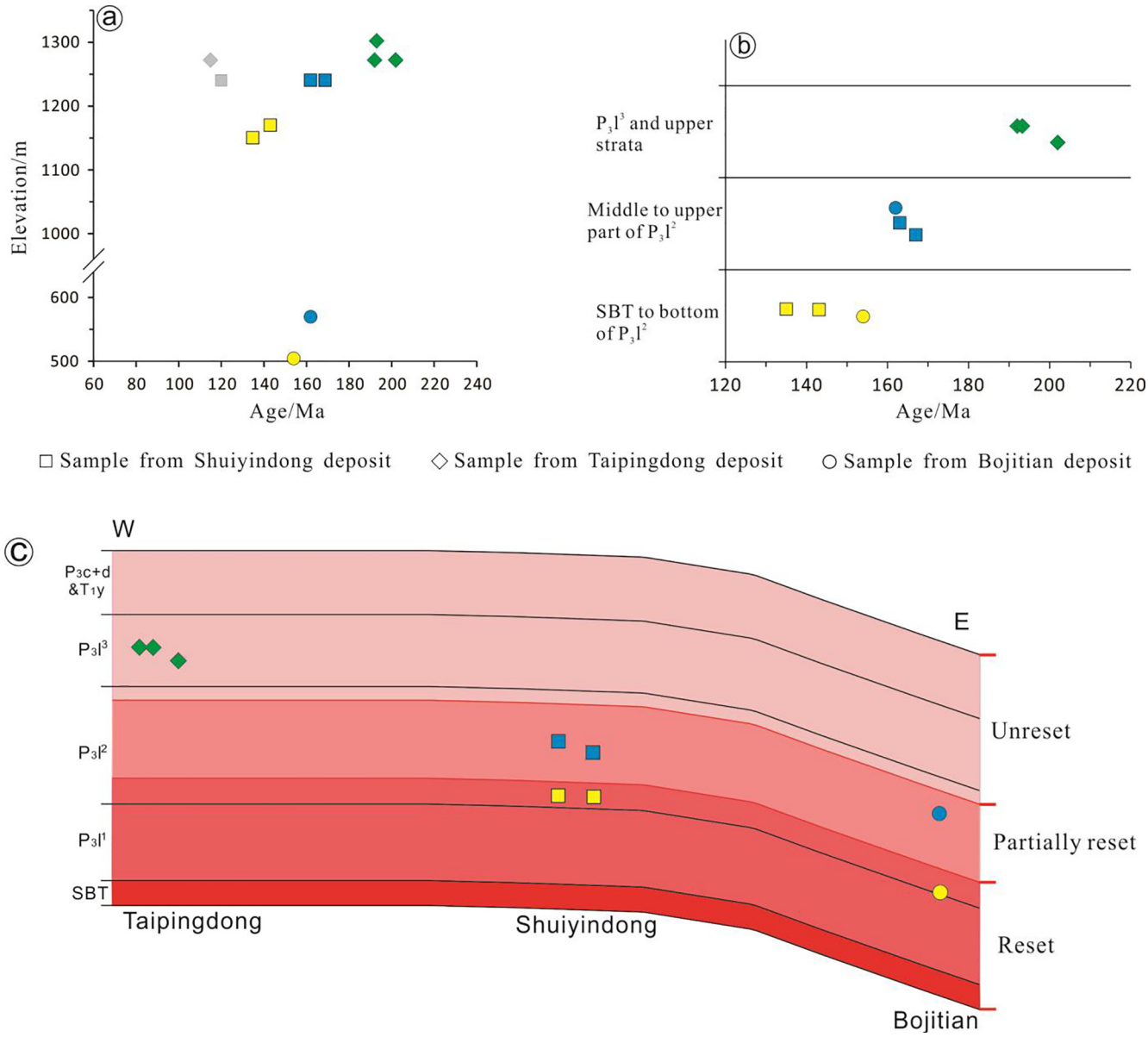

Fig. 5. The spatial distribution of zircon fission track ages in the Huijiabao anticline. (a) age-elevation plot of zircon fission track central ages of samples with exact sampling locations from the Shuiyindong, Taipingdong and Bojitian deposits. (b) The corresponding relationship between zircon fission track central ages and stratigraphic sequences. (c) A conceptual diagram showing the effect of hydrothermal reset on zircon fission track. The yellow data points represent samples which were completely reset during mineralization and recorded the mineralization age (132–160 Ma). The green data points represent samples which were unreset during mineralization and recorded the age of the Indosinian orogeny (192–216 Ma). The blue data points represent samples which were partially reset during mineralization and recorded both the ages of mineralization and the Indosinian orogeny. The light grey data points represent SYD-5 and TPD-7 samples, which have very high average U content. The stratigraphic sequences in (b) and (c) are consistent with Fig. 3a. (For interpretation of the references to colour in this figure legend, the reader is referred to the web version of this article.)

difference is only 150 m, and the corresponding geothermal difference is only about 4.5 °C. Such a limited difference in elevation and geothermal temperature is unlikely to result in an age difference of about 60 Myr in the process of uplift and exhumation. (2) The distance between Bojitian and Shuiyindong deposits is only about 4 km (Fig. 2a), and the vertical dislocations of faults between them are less than 100 m (Xia, 2005). In this case, samples from the Bojitian and Shuiyindong deposits should fall roughly on the same line in the age-elevation plot if only uplift and exhumation process is considered. However, it is inconsistent with the facts shown in Fig. 5a. Therefore, both reasons above suggest some other processes lead to the trend of age increasing with elevation in the Shuiyindong and Taipingdong deposits, and in the Bojitian deposit.

It is worth to note that there is a corresponding relationship between sample fission track ages and stratigraphic sequences (Fig. 5b): Firstly, the samples of SYD2-8, SYD2-9 and BJT-2 collected from the bottom of the second unit of the Longtan Formation (bottom of P_3l^2) yielded ages of 135–154 Ma, which record the mineralization age. Secondly, the samples of SYD-6, SYD-7 and BJT-1 collected from the middle to upper part of the second unit of the Longtan Formation (middle to upper part of P_3l^2) yielded fission track central ages of 162–167 Ma. However, all of their P(χ^2) are less than 5%, and each of them can be decomposed into two components with ages of ~140 Ma and ~210 Ma, respectively (Table 3). Therefore, both the mineralization age (~140 Ma) and the cooling age of the Indosinian orogeny thermal events (~210 Ma) were recorded by the three samples. Thirdly, the samples of TPD-8, TPD-9 and TPD-10 collected from the third unit of the Longtan Formation (P_3l^3) yielded ages of 192–202 Ma, which

only record the cooling age of the Indosinian orogeny thermal events.

As the reset of zircon fission track requires a temperature above the closure temperature and a sufficient time of duration, one possible explanation for the age-stratigraphic correspondence is the decrease of temperature and duration of hydrothermal activity from lower to upper stratigraphic sequence. Specifically, in the core of the Huijiabao anticline, the unconformity interface (SBT) between the Middle Permian Maokou Formation and the Upper Permian Longtan Formation was the migration channel of ore-forming fluids (Liu et al., 2002; Liu, et al., 2006; Su et al., 2009a; Chen et al., 2015). During mineralization, after starting from SBT, the fluid flowed and permeated from lower to upper strata along interlayer faults, which may cause the temperature of fluid in lower strata to be higher than that in upper strata. More importantly, with the weakening of hydrothermal activity, the area of fluid activity may be narrowed to lower strata, which may lead to the duration of hydrothermal activity in lower strata being longer than that in upper strata. From SBT to the bottom of the second unit of the Longtan Formation (SBT to bottom of P_3l^2), the high fluid temperature and long hydrothermal duration would reset all zircon fission tracks in the strata, which could well record the mineralization age (Fig. 5b, c). In contrast, in the third unit of the Longtan Formation and upper strata (P_3l^3 and upper strata), zircon fission tracks could not be reset due to low fluid temperature and short hydrothermal duration, so that these zircons still record the Indosinian orogeny thermal event (Fig. 5b, c). Besides, in the middle to upper part of the second unit of the Longtan Formation (middle to upper part of P_3l^2), the temperature and duration of the fluid were only enough to make the zircon components with high radiation damage to be reset to record the age of mineralization, while the zircon components with low radiation damage were not reset and still record the Indosinian orogeny thermal event (Fig. 5b, c).

This interpretation can be supported by the spatial distribution of metallogenic elements. Tan et al. (2015) studied the distribution of elements in a section of the Shuiyindong deposit. The results show that Au deposited during the main metallogenic stage can be enriched in the second and third units of the Longtan Formation, while As, Sb, Hg and Tl generally deposited during the late metallogenic stage are mainly concentrated in the SBT and the first unit of the Longtan Formation. It indicates that hydrothermal activity in lower strata had a longer duration.

5.5. The fission track age of zircons with abnormally high U content records the mafic magmatic thermal event in southwestern Guizhou

The zircons with abnormally high U content in TPD-7 sample obtained fission track age of 88 Ma (Table 3; Fig. 4), which is consistent with the age of 84–88 Ma of the mafic dykes intruded into Lurong-Baiceng area in southwestern Guizhou (Figs. 1c and 2a; Chen et al., 2009b; Liu et al., 2010). Therefore, this zircon fission track age may be a record of this post-ore magmatic thermal event. Because these dykes are small and far away (> 15 km) from the Carlin-type gold deposits in this study, their thermal influence was limited, and only a few zircons with high U and high radiation damage (thus low closure temperature) have recorded this event.

5.6. Apatite fission track ages record a lower temperature hydrothermal activity in the Cenozoic

Because the closure temperature of apatite fission track is very low (90–120 °C; Ketcham et al., 1999), it is easy to be disturbed by later thermal events. The fission track ages of seven apatite samples from Shuiyindong, Taipingdong and Getang deposits are young and concentrate in 19–40 Ma (Fig. 4d). These ages are significantly younger than the apatite fission track ages of the corresponding strata in the region (56, 57 and 91 Ma; Qiu et al., 2016). Therefore, they should not be the record of the cooling history related to regional uplift and exhumation. Instead, these apatite fission track ages probably record a lower temperature thermal event in the Cenozoic. Recently, Huang et al. (2012) reported a Sm-Nd isochron age of 35.8 ± 0.9 Ma for hydrothermal fluorites from the Getang gold deposit. This age is consistent with the apatite fission track ages in this study, indicating that hydrothermal superimposition may have occurred during this period. The temperature range of this superimposed hydrothermal activity is speculated to be 120–170 °C, because it could only reset fission track in apatite but was not recorded by zircon (U-Th)/He and fission track systems. Furthermore, this period of hydrothermal activity was recorded by apatites from three deposits on a regional scale, suggesting this activity was extensive in southwestern Guizhou although its temperature was relatively low.

6. Conclusion

(1) Zircon fission track, zircon (U-Th)/He and apatite fission track techniques were applied to the Carlin-type gold deposits in southwestern Guizhou. Four groups of ages were obtained, i.e., 192–216 Ma, 132–160 Ma, 88 Ma and 19–40 Ma. These ages are probably the records of four geological thermal events in southwestern Guizhou.
(2) Low-temperature thermochronological constraints, combined with field relationships, indicate that the Carlin-type gold deposits in southwestern Guizhou most likely formed at 132–160 Ma.
(3) The ages of 192–216 Ma, 88 Ma and 19–40 Ma may record the tectonic thermal event caused by the Indosinian orogeny, the magmatic thermal event related to the intrusion of local mafic dykes, and a lower temperature but extensive hydrothermal superimposition in southwestern Guizhou, respectively.
(4) The spatial distribution of zircon fission track ages in the Huijiabao anticline reflects the decrease of temperature and duration of hydrothermal activity from lower to upper stratigraphic sequences.

Acknowledgements

It is a great honor to dedicate this article to Academician Yusheng Zhai on the occasion of his 90th birthday. This work was financially supported by the projects of National Natural Science Foundation of China (41830432, U1812402) and the National 973 Project of China (2014CB440900). We are grateful to Guizhou Zijin Mining Co., Ltd., Guizhou Huajin Mining Co., Ltd. and Southwest Guizhou Jinlong Gold Mining Co., Ltd. for access to samples. Prof. Xingchun Zhang, Dr. Chengfu Yang, Dr. Rui Liu, Dr. Heqing Liu and Dr. Chaofei Zheng are thanked for their help during fieldwork. We would like to thank Prof. Qi Zhou, Prof. Wenchao Su and Prof. Jiafei Xiao for their constructive suggestions. We are grateful to Prof. Wanming Yuan and Prof. Peter W. Reiners for their help with fission track analysis and (U-Th)/He analysis, respectively. We also acknowledge constructive comments from Prof. Qingfei Wang and an anonymous reviewer and editorial handling by Prof. Franco Pirajno and Prof. Liqiang Yang.

References

Arehart, G.B., Chakurian, A.M., Tertbar, D.R., Christensen, J.N., McInnes, B.A., Donelick, R.A., 2003. Evaluation of radioisotope dating of Carlin-type deposits in the Great Basin, western North America, and implications for deposit genesis. Econ. Geol. 98, 235–248.
Arehart, G.B., Donelick, R.A., 2006. Thermal and isotopic profiling of the Pipeline hydrothermal system: Application to exploration for Carlin-type gold deposits. J. Geochem. Explor. 91, 27–40.
Arehart, G.B., Foland, K.A., Naeser, C.W., Kesler, S.E., 1993. Ar^{40}/Ar^{39}, K/Ar, and fission-track geochronology of sediment-hosted disseminated gold deposits at Post-Betze, Carlin trend, northeastern Nevada. Econ. Geol. 88, 622–646.
Ashley, R.P., Cunningham, C.G., Bostick, N.H., Dean, W.E., Chou, I.M., 1991. Geology and geochemistry of three sedimentary-rock-hosted disseminated gold deposits in Guizhou Province, People's Republic of China. Ore Geol. Rev. 6, 133–151.
Bellemans, F., Decorte, F., Vandenhaute, P., 1995. Composition of srm and cn u-doped glasses: Significance for their use as thermal neutron fluence monitors in fission track dating. Radiat. Meas. 24, 153–160.

Bernet, M., Garver, J.I., 2005. Fission-track analysis of detrital zircon. Rev. Mineral. Geochem. 58, 205–237.
Betsi, T.B., Lentz, D., McInnes, B., Evans, N.J., 2012. Emplacement ages and exhumation rates for intrusion-hosted Cu-Mo-Sb-Au mineral systems at Freegold Mountain (Yukon, Canada): assessment from U-Pb, Ar-Ar, and (U-Th)/He geochronometers. Can. J. Earth Sci. 49, 653–670.
Brandon, M.T., 2002. Decomposition of mixed grain age distributions using Binomfit. On Track 24, 13–18.
Brandon, M.T., Roden-Tice, M.K., Garver, J.I., 1998. Late Cenozoic exhumation of the Cascadia accretionary wedge in the Olympic Mountains, northwest Washington State. Geol. Soc. Am. Bull. 110, 985–1009.
Cai, J.X., Zhang, K.J., 2009. A new model for the Indochina and South China collision during the Late Permian to the Middle Triassic. Tectonophysics 467, 35–43.
Carter, A., 1990. The thermal history and annealing effects in zircons from the Ordovician of North Wales. Int. J. Radiat. Appl. Instrum. Part D: Nucl. Tracks Radiat. Meas. 17, 309–313.
Chakurian, A.M., Arehart, G.B., Donelick, R.A., Zhang, X., Reiners, P.W., 2003. Timing constraints of gold mineralization along the Carlin trend utilizing apatite fission-track, $^{40}Ar/^{39}Ar$, and apatite (U-Th)/He methods. Econ. Geol. 98, 1159–1171.
Chen, M.H., Mao, J.W., Qu, W.J., Wu, L.L., Uttley, P.J., Norman, T., Zheng, J.M., Qin, Y.Z., 2007. Re-Os dating of arsenian pyrites from the Lannigou gold deposit, Zhenfeng, Guizhou Province, and its geological significances. Geol. Rev. 53, 371–382 (in Chinese with English abstract).
Chen, M.H., Huang, Q.W., Hu, Y., Chen, Z.Y., Zhang, W., 2009a. Genetic types of phyllosilicate (mica) and its ^{39}Ar–^{40}Ar dating in Lannigou gold deposit, Guizhou province, China. Acta Mineral. Sinica 29, 353–362 (in Chinese with English abstract).
Chen, M.H., Mao, J.W., Li, C., Zhang, Z.Q., Dang, Y., 2015. Re-Os isochron ages for arsenopyrite from Carlin-like gold deposits in the Yunnan-Guizhou-Guangxi "golden triangle", southwestern China. Ore Geol. Rev. 64, 316–327.
Chen, M.H., Bagas, L., Liao, X., Zhang, Z.Q., Li, Q.L., 2019. Hydrothermal apatite SIMS Th-Pb dating: Constraints on the timing of low-temperature hydrothermal Au deposits in Nibao, SW China. Lithos 324–325, 418–428.
Chen, F., Yan, D.P., Yang, W.X., Qiu, L., Dong, J.M., 2017. Metallogenic structure of the Shuiyindong deposit in the Youjiang basin and its indication for gold enrichment. Annual Meeting of Chinese Geosciences Union. Chinese Geophysical Society, Beijing October 15, 2017. Poster presentation (in Chinese).
Chen, M.H., Zhang, W., Yang, Z.X., Lu, G., Hou, K.J., Liu, J.H., 2009b. Zircon SHRIMP U-Pb age and Hf isotopic composition of Baiceng ultrabasic dykes in Zhenfeng County, southwestern Guizhou Province. Miner. Deposits 28, 240–250 (in Chinese with English abstract).
Cline, J.S., Hofstra, A.H., Muntean, J.L., Tosdal, R.M., Hickey, K.A., 2005. Carlin-type gold deposits in Nevada: Critical geologic characteristics and viable models. Econ. Geol., 100th anniversary volume, 451–484.
Cunningham, C.G., Ashley, R.P., Chou, I.M., Huang, Z.S., Wan, C.Y., Li, W.K., 1988. Newly discovered sedimentary rock-hosted disseminated gold deposits in the People's Republic of China. Econ. Geol. 83, 1462–1467.
Cunningham, C.G., Austin, G.W., Naeser, C.W., Rye, R.O., Ballantyne, G.H., Stamm, R.G., Barker, C.E., 2004. Formation of a paleothermal anomaly and disseminated gold deposits associated with the Bingham Canyon Porphyry Cu-Au-Mo system, Utah. Econ. Geol. 99, 789–806.
Deng, J., Yuan, W.M., Carranza, E.J.M., Yang, L.Q., Wang, C.M., Yang, L.Y., Hao, N.N., 2014. Geochronology and thermochronometry of the Jiapigou gold belt, northeastern China: New evidence for multiple episodes of mineralization. J. Asian Earth Sci. 89, 10–27.
Du, Y.S., Huang, H., Yang, J.H., Huang, H.W., Tao, P., Huang, Z.Q., Hu, L.S., Xie, C.X., 2013. The basin translation from Late Paleozoic to Triassic of the Youjiang basin and its tectonic signification. Geol. Rev. 59, 1–11 (in Chinese with English abstract).
Farley, K.A., 2002. (U-Th)/He dating: Techniques, calibrations, and applications. Rev. Mineral. Geochem. 47, 819–844.
Fitzgerald, P.G., Baldwin, S.L., Webb, L.E., O'Sullivan, P.B., 2006. Interpretation of (U-Th)/He single grain ages from slowly cooled crustal terranes: A case study from the Transantarctic Mountains of southern Victoria Land. Chem. Geol. 225, 91–120.
Fu, S.L., Hu, R.Z., Batt, G.E., Danisik, M., Evans, N.J., Mi, X.F., 2019a. Zircon (U-Th)/He thermochronometric constraints on the mineralization of the giant Xikuangshan Sb deposit in central Hunan, South China. Mineral. Deposita.
Fu, S.L., Hu, R.Z., Yan, J., Lan, Q., Gao, W., 2019b. The mineralization age of the Banxi Sb deposit in Xiangzhong metallogenic province of southern China. Ore Geol. Rev. 112, 103033.
Galbraith, R.F., 1981. On statistical-models for fission-track counts. J. Int. Assoc. Math. Geol. 13, 471–478.
Galbraith, R.F., Green, P.F., 1990. Estimating the component ages in a finite mixture. Nucl. Tracks Radiat. Meas. 17, 197–206.
Galbraith, R.F., Laslett, G.M., 1993. Statistical models for mixed fission track ages. Nucl. Tracks Radiat. Meas. 21, 459–470.
Garver, J.I., Riley, B.C.D., Wang, G., 2002. Partial resetting of fission tracks in detrital zircon. European Fission-Track Conference, Cadiz, Spain. Geotemas 4, 73–75.
Garver, J.I., Reiners, P.W., Walker, L.J., Ramage, J.M., Perry, S.E., 2005. Implications for timing of Andean uplift from thermal resetting of radiation-damaged zircon in the Cordillera Huayhuash, northern Peru. J. Geol. 113, 117–138.
Gleadow, A.J.W., Duddy, I.R., Green, P.F., Lovering, J.F., 1986. Confined fission-track lengths in apatite: a diagnostic tool for thermal history analysis. Contrib. Miner. Petrol. 94, 405–415.
Green, P.F., 1981. A new look at statistics in fission-track dating. Nucl. Tracks 5, 77–86.
Green, P.F., Duddy, I.R., Gleadow, A.J.W., Tingate, P.R., Laslett, G.M., 1986. Thermal annealing of fission tracks in apatite: 1. A qualitative description. Chem. Geol.: Isotope Geosci. Section 59, 237–253.
Gu, X.X., Zhang, Y.M., Li, B.H., Dong, S.Y., Xue, C.J., Fu, S.H., 2012. Hydrocarbon and ore-bearing basinal fluids: a possible link between gold mineralization and hydrocarbon accumulation in the Youjiang basin, South China. Miner. Deposita 47, 663–682.
Guizhou Institute of Geological Survey, 2017. The regional geology of China, Guizhou province. Geological Publishing House, Beijing, pp. 1–1153 (in Chinese).
Han, Z.J., Wang, Y.G., Feng, J.Z., Chen, T.J., Luo, X.H., Liu, Y.H., 1999. The geology and exploration of gold deposits in southwestern Guizhou. Guizhou Science and Technology Press, Guiyang, pp. 1–146 (in Chinese with English abstract).
He, B., Xu, Y.G., Chung, S.L., Xiao, L., Wang, Y., 2003. Sedimentary evidence for a rapid, kilometer-scale crustal doming prior to the eruption of the Emeishan flood basalts. Earth Planet. Sci. Lett. 213, 391–405.
Hofstra, A.H., Cline, J.S., 2000. Characteristics and models for Carlin-type gold deposits. Rev. Econ. Geol. 13, 163–220.
Hofstra, A.H., Snee, L.W., Rye, R.O., Folger, H.W., Phinisey, J.D., Loranger, R.J., Dahl, A.R., Naeser, C.W., Stein, H.J., Lewchuk, M.T., 1999. Age constraints on Jerritt Canyon and other carlin-type gold deposits in the Western United States; relationship to mid-Tertiary extension and magmatism. Econ. Geol. 94, 769–802.
Hu, R.Z., Su, W.C., Bi, X.W., Tu, G.C., Hofstra, A.H., 2002. Geology and geochemistry of Carlin-type gold deposits in China. Miner. Deposita 37, 378–392.
Hu, R.Z., Peng, J.T., Ma, D.S., Su, W.C., Shi, C.H., Bi, X.W., Tu, G.C., 2007. Epoch of large-scale low-temperature mineralizations in southwestern Yangtze massif. Miner. Deposits 26, 583–596 (in Chinese with English abstract).
Hu, R.Z., Zhou, M.F., 2012. Multiple Mesozoic mineralization events in South China-an introduction to the thematic issue. Miner. Deposita 47, 579–588.
Hu, R.Z., Mao, J.W., Hua, R.M., Fan, W.M., 2015. Intra-continental mineralization of South China Craton. Science Press, Beijing, pp. 1–903 (in Chinese).
Hu, R.Z., Chen, W.T., Xu, D.R., Zhou, M.F., 2017a. Reviews and new metallogenic models of mineral deposits in South China: An introduction. J. Asian Earth Sci. 137, 1–8.
Hu, R.Z., Fu, S.L., Huang, Y., Zhou, M.F., Fu, S.H., Zhao, C.H., Wang, Y.J., Bi, X.W., Xiao, J.F., 2017b. The giant South China Mesozoic low-temperature metallogenic domain: Reviews and a new geodynamic model. J. Asian Earth Sci. 137, 9–34.
Huang, J.G., Li, H.J., Li, W.J., Dong, L., 2012. Trace element characteristics of fluorite and its Sm-Nd isotopic dating in Getang gold deposit, Guizhou province. Adv. Earth Sci. 27, 1087–1093 (in Chinese with English abstract).
Hurford, A.J., 1990. Standardization of fission track dating calibration: Recommendation by the Fission Track Working Group of the I.U.G.S. Subcommission on Geochronology. Chem. Geol.: Isotope Geosci. Sect. 80, 171–178.
Hurford, A.J., Green, P.F., 1982. A users' guide to fission track dating calibration. Earth Planet. Sci. Lett. 59, 343–354.
Kesler, S.E., Riciputi, L.C., Ye, Z.J., 2005. Evidence for a magmatic origin for Carlin-type gold deposits: isotopic composition of sulfur in the Betze-Post-Screamer deposit, Nevada, USA. Miner. Deposita 40, 127–136.
Ketcham, R.A., Donelick, R.A., Carlson, W.D., 1999. Variability of apatite fission-track annealing kinetics: III. extrapolation to geological time scales. Am. Mineral. 84, 1235–1255.
Laubacher, G., Naeser, C.W., 1994. Fission-track dating of granitic-rocks from the eastern Cordillera of Peru: Evidence for late Jurassic and Cenozoic cooling. J. Geol. Soc. 151, 473–483.
Liu, J.Z., 2001. The geology of the Yanshang gold deposit, Zhenfeng county, Guizhou. Guizhou Geol. 18, 174–178 (in Chinese with English abstract).
Liu, J.Z., Deng, Y.M., Liu, C.Q., Zhang, X.C., Xia, Y., 2006. Metallogenic conditions and model of the super large Shuiyindong stratabound gold deposit in Zhenfeng County, Guizhou Province. Geol. China 33, 169–177 (in Chinese with English abstract).
Liu, J.Z., Chen, J.H., Deng, Y.M., Fu, Z.K., Chen, F.E., You, B., 2009. Exploration of the Shuiyingdong super-scale gold deposit and the evolution of exploration for metallogenic belt of the Huijiabao anticline in Guozhou Province. Geol. Surv. Res. 32, 138–143 (in Chinese with English abstract).
Liu, X., Fan, H.R., Evans, N.J., Yang, K.F., Danišík, M., McInnes, B.I.A., Qin, K.Z., Yu, X.F., 2017. Exhumation history of the Sanshandao Au deposit, Jiaodong: constraints from structural analysis and (U-Th)/He thermochronology. Sci. Rep. 7, 1–12.
Liu, S., Su, W.C., Hu, R.Z., Feng, C.X., Gao, S., Coulson, I.M., Wang, T., Feng, G.Y., Tao, Y., Xia, Y., 2010. Geochronological and geochemical constraints on the petrogenesis of alkaline ultramafic dykes from southwest Guizhou Province, SW China. Lithos 114, 253–264.
Liu, J.M., Ye, J., Ying, H.L., Liu, J.J., Zheng, M.H., Gu, X.X., 2002. Sediment-hosted micro-disseminated gold mineralization constrained by basin paleo-topographic highs in the Youjiang basin, South China. J. Asian Earth Sci. 20, 517–533.
Long, A., Rippeteau, B., 1974. Testing Contemporaneity and Averaging Radiocarbon Dates. Am. Antiq. 39, 205–215.
Mao, S.H., 1991. Occurrence and distribution of invisible gold in a Carlin-type gold deposit in China. Am. Mineral. 76, 1964–1972.
Marton, I., 2015. Hydrothermal Ores (Thermochronology). In: Encyclopedia of Scientific Dating Methods. Springer, pp. 334–339.
Marton, I., Moritz, R., Spikings, R., 2010. Application of low-temperature thermochronology to hydrothermal ore deposits: Formation, preservation and exhumation of epithermal gold systems from the Eastern Rhodopes, Bulgaria. Tectonophysics 483, 240–254.
McInnes, B.I.A., Evans, N.J., Fu, F.Q., Garwin, S., 2005. Application of thermochronology to hydrothermal ore deposits. Rev. Mineral. Geochem. 58, 467–498.
Muntean, J.L., Cline, J.S., Simon, A.C., Longo, A.A., 2011. Magmatic-hydrothermal origin of Nevada's Carlin-type gold deposits. Nat. Geosci. 4, 122–127.
Peng, Y.W., Gu, X.X., Zhang, Y.M., Liu, L., Wu, C.Y., Chen, S.Y., 2014. Ore-forming process of the Huijiabao gold district, southwestern Guizhou Province, China: Evidence from fluid inclusions and stable isotopes. J. Asian Earth Sci. 93, 89–101.
Peters, S.G., Huang, J.Z., Li, Z.P., Jing, C.G., 2007. Sedimentary rock-hosted Au deposits

of the Dian–Qian–Gui area, Guizhou, and Yunnan Provinces, and Guangxi District, China. Ore Geol. Rev. 31, 170–204.
Pi, Q.H., Hu, R.Z., Bi, X.W., Peng, K.Q., Wu, J.B., Wei, Z.W., Huang, Y., 2016. Geochronology of the Zhesang gold deposit and mafc rock in Funing County of Yunnan Province, with special reference to the dynamic background of Carlin-type gold deposits in the Dian-Qian-Gui region. Acta Petrol. Sinica 32, 3331–3342 (in Chinese with English abstract).
Pi, Q.H., Hu, R.Z., Xiong, B., Li, Q.L., Zhong, R.C., 2017. In situ SIMS U-Pb dating of hydrothermal rutile: reliable age for the Zhesang Carlin-type gold deposit in the golden triangle region, SW China. Miner. Deposita 52, 1179–1190.
Qiu, L., Yan, D.P., Tang, S.L., Wang, Q., Yang, W.X., Tang, X.L., Wang, J.B., 2016. Mesozoic geology of southwestern China: Indosinian foreland overthrusting and subsequent deformation. J. Asian Earth Sci. 122, 91–105.
Rahn, M.K., Brandon, M.T., Batt, G.E., Garver, J.I., 2004. A zero-damage model for fission-track annealing in zircon. Am. Mineral. 89, 473–484.
Regional Geological Survey Team of Guizhou Geological Bureau, 1981. 1: 200000 Geological map of the People's Republic of China, sheet Xingren (G-48-XXII).
Reiners, P.W., 2005. Zircon (U-Th)/He thermochronometry. Rev. Mineral. Geochem. 58, 151–179.
Reiners, P.W., Spell, T.L., Nicolescu, S., Zanetti, K.A., 2004. Zircon (U-Th)/He thermochronometry: He diffusion and comparisons with $^{40}Ar/^{39}Ar$ dating. Geochim. Cosmochim. Acta 68, 1857–1887.
Reiners, P.W., Ehlers, T.A., Zeitler, P.K., 2005. Past, present, and future of thermochronology. Rev. Mineral. Geochem. 58, 1–18.
Seward, D., Rhoades, D.A., 1986. A clustering technique for fission-track dating of fully to partially annealed minerals and other nonunique populations. Nucl. Tracks Radiat. Meas. 11, 259–268.
Su, W.C., Xia, B., Zhang, H.T., Zhang, X.C., Hu, R.Z., 2008. Visible gold in arsenian pyrite at the Shuiyindong Carlin-type gold deposit, Guizhou, China: Implications for the environment and processes of ore formation. Ore Geol. Rev. 33, 667–679.
Su, W.C., Heinrich, C.A., Pettke, T., Zhang, X.C., Hu, R.Z., Xia, B., 2009a. Sediment-hosted gold deposits in Guizhou, China: products of wall-rock sulfidation by deep crustal fluids. Econ. Geol. 104, 73–93.
Su, W.C., Hu, R.Z., Xia, B., Xia, Y., Liu, Y.P., 2009b. Calcite Sm-Nd isochron age of the Shuiyindong Carlin-type gold deposit, Guizhou, China. Chem. Geol. 258, 269–274.
Su, W.C., Dong, W.D., Zhang, X.C., Shen, N.P., Hu, R.Z., Hofstra, A.H., Cheng, L.Z., Xia, Y., Yang, K.Y., 2018. Carlin-Type Gold Deposits in the Dian-Qian-Gui "Golden Triangle" of Southwest China. Rev. Econ. Geol. 20, 157–185.
Suo, S.T., Bi, X.M., Zhao, W.X., Hou, G.J., 1998. Very low-grade metamorphism and its geodynamical significance of Triassic strata within the Youjiang river basin. Sci. Geol. Sinica 33, 395–405 (in Chinese with English abstract).
Tan, Q.P., Xia, Y., Xie, Z.J., Yan, J., 2015. Migration paths and precipitation mechanisms of ore-forming fluids at the Shuiyindong Carlin-type gold deposit, Guizhou, China. Ore Geol. Rev. 69, 140–156.
Tretbar, D.R., Arehart, G.B., Christensen, J.N., 2000. Dating gold deposition in a Carlin-type gold deposit using Rb/Sr methods on the mineral galkhaite. Geology 28, 947–950.
Wang, Z.S., 1997. Affrmation of the Jurassic in Longtoushan of Zhenfeng, Guizhou and its geological significance. Guizhou Geol. 14, 201–203 (in Chinese with English abstract).
Wang, Z.P., 2013. Genesis and dynamic mechanism of the epithermal ore deposits, SW Guizhou, China. A case study of gold and antimony deposits (PhD thesis). Institute of Geochemistry, Chinese Academy of Sciences, Guiyang, pp. 1–150 (in Chinese with English abstract).
Wang, Y.G., Suo, S.T., Zhang, M.F., 1994. Tectonics and Carlin-type gold deposits in southwestern Guizhou. Geological Publishing House, Beijing, pp. 1–155.
Wang, Y.G., Wang, L.T., Zhang, M.F., Wang, L.L., 1995. Texture of the upper crust and pattern of the disseminated gold deposits distributed in Nanpanjiang area. Guizhou Geol. 12, 91–183 (in Chinese with English abstract).
Wilk, M.B., Gnanadesikan, R., 1968. Probability plotting methods for the analysis for the analysis of data. Biometrika 55, 1–17.
Wolff, R., Dunkl, I., Kempe, U., Eynatten, H.V., 2015. The Age of the Latest Thermal Overprint of Tin and Polymetallic Deposits in the Erzgebirge, Germany: Constraints from Fluorite (U-Th-Sm)/He Thermochronology. Econ. Geol. 110, 2025–2040.
Xia, Y., 2005. Characteristics and model for Shuiyindong gold deposit in southwestern Guizhou, China (PhD thesis). Institute of Geochemistry, Chinese Academy of Sciences, Guiyang, pp. 1–123 (in Chinese with English abstract).
Yang, J.H., Cawood, P.A., Du, Y.S., Huang, H., Hu, L.S., 2012. Detrital record of Indosinian mountain building in SW China: Provenance of the Middle Triassic turbidites in the Youjiang Basin. Tectonophysics 574, 105–117.
Yuan, W.M., Bao, Z.K., Dong, J.Q., Guo, Z.J., Deng, J., 2007. Zircon and apatite fission track analyses on mineralization ages and tectonic activities of Tuwu-Yandong porphyry copper deposit in northern Xinjiang, China. Sci. China Series D-Earth Sci. 50, 1787–1795.
Yuan, W.M., Zheng, Q.G., Bao, Z.K., Dong, J.Q., Carter, A., An, Y.C., Deng, J., 2009. Zircon fission track thermochronology constraints on mineralization epochs in Altai Mountains, northern Xinjiang, China. Radiat. Meas. 44, 950–954.
Yuan, W.M., Mo, X.X., Zhang, A.K., Chen, X.N., Duan, H.W., Li, X., Hao, N.N., Wang, X.M., 2013. Fission Track Thermochronology Evidence for Multiple Periods of Mineralization in the Wulonggou Gold Deposits, Eastern Kunlun Mountains, Qinghai Province. J. Earth Sci. 24, 471–478.
Zhang, X.C., Spiro, B., Halls, C., Stanley, C.J., Yang, K.Y., 2003. Sediment-hosted disseminated gold deposits in Southwest Guizhou, PRC: their geological setting and origin in relation to mineralogical, fluid inclusion, and stable-isotope characteristics. Int. Geol. Rev. 45, 407–470.
Zhang, X.C., Hofstra, A.H., Hu, R.Z., Emsbo, P., Su, W.C., Ridley, W.I., 2005. Geochemistry and $\delta^{34}S$ of ores and ore stage iron sulfides in Carlin-type gold deposits, Dian-Qian-Gui area, China: Implications for ore genesis. In: Mineral Deposit Research: Meeting the Global Challenge. Springer Berlin Heidelberg, pp. 1107–1110.
Zhao, J.X., Qin, K.Z., Li, G.M., Cao, M.J., Evans, N.J., McInnes, B.I.A., Li, J.X., Xiao, B., Chen, L., 2015. The exhumation history of collision-related mineralizing systems in Tibet: Insights from thermal studies of the Sharang and Yaguila deposits, central Lhasa. Ore Geol. Rev. 65, 1043–1061.
Zheng, Q.Q., Zhang, M.F., Cheng, D.Q., Che, Z., Wang, C.H., Dai, C.G., 1989. Ore-controlling conditions of micro-grained gold deposits in southwestern Guizhou. In: Collected works of regional ore-forming condition of main gold deposit styles in China, v. 6. Southern Guizhou. Geological Publishing House, Beijing, pp. 87–113 (in Chinese).
Zhou, X.Y., 1990. The Ordovician-Triassic conodont colour alteration index (CAI) and evaluation of hydrocarbon in Guizhou. Geol. Guizhou 7, 361–372 (in Chinese with English abstract).
Zhuang, X.G., 1995. The paleogeothermal field of northwestern Guangxi: Characteristics and its role in the formation of micro-disseminated gold deposits. Miner. Deposits 14, 82–89 (in Chinese with English abstract).